Organic & Biomolecular Chemistry

RSC Publishing

PAPER

# Determination of the binding epitope of RGD-peptidomimetics to $\alpha_v\beta_3$ and $\alpha_{IIb}\beta_3$ integrin-rich intact cells by NMR and computational studies†

Cite this: *Org. Biomol. Chem.*, 2013, **11**, 3886

Ileana Guzzetti,[a] Monica Civera,[a] Francesca Vasile,[a] Elena M. Araldi,[a] Laura Belvisi,*[a,b] Cesare Gennari,[a,b] Donatella Potenza,*[a,b] Roberto Fanelli[c] and Umberto Piarulli[c]

Received 18th March 2013,
Accepted 18th April 2013

DOI: 10.1039/c3ob40540k

**www.rsc.org/obc**

NMR experiments (transferred NOE and Saturation Transfer Difference) were used to shed light on the binding epitope of RGD peptidomimetics **1–3** with integrins $\alpha_v\beta_3$ and $\alpha_{IIb}\beta_3$, expressed on the membrane of ECV304 bladder cancer cells and human platelets, respectively. The NMR results were supported by docking calculations of **1–3** in the active sites of $\alpha_v\beta_3$ and $\alpha_{IIb}\beta_3$ integrin receptors and were compared to the results of competitive $\alpha_v\beta_3$ receptor binding assays and competitive ECV304 cell adhesion experiments. While *cis* RGD ligand **1** interacts mainly with the α integrin subunit through its basic guanidine group, *trans* RGD ligands **2** and **3** are able to interact with both the α and β integrin subunits *via* an electrostatic clamp.

## Introduction

The understanding of the interaction of a protein with its ligands requires precise knowledge about the underlying recognition events at a molecular level. A variety of biophysical methods have been developed for this purpose and, recently, several novel NMR spectroscopic techniques have emerged as powerful tools to identify and characterize the binding epitope of ligands to receptor proteins.[1] Among these, transferred NOE (tr-NOE) has gained momentum, as it provides the basis for a variety of experimental protocols that are designed to detect and characterize binding activity.[2] The observation of tr-NOEs relies on the different behaviour of a small ligand molecule free in solution rather than bound to a receptor protein. In fact, a ligand bound to a large-molecular weight protein behaves as a part of the large molecule and adopts the corresponding NOE behaviour, showing strong negative NOEs, so-called tr-NOEs. These tr-NOEs reflect the bound conformation of the ligand. Binding of a ligand to a receptor protein can thus easily be distinguished by looking at the sign and size of the observed NOEs. A NMR spectroscopic technique, complementary to tr-NOE, is Saturation Transfer Difference (STD).[1b,3] This sequence helps identifying the group epitope, revealing which moieties of the ligand molecule are closest to the receptor in the bound state. The method is based on the transfer of saturation from the protein to the bound ligand which, by exchange, is released into solution where it is detected. The degree of saturation of individual ligand protons (expressed as absolute-STD percent) reflects their proximity to the protein surface and can be used to describe the ligand–target interactions.

Recently, our group has applied these methodologies using intact tumor cells[4] or platelets[5] to investigate the ligand–receptor interactions between azabicyclic lactam peptidomimetic ligands containing the Arg–Gly–Asp (RGD) recognition sequence and $\alpha_v\beta_3$ and $\alpha_{IIb}\beta_3$ integrin target proteins. Integrins are a large family of transmembrane heterodimeric glycoprotein receptors, composed of two non-covalently associated α and β subunits.[6] As a consequence of their role in important physiological phenomena, integrin defects have been implicated in many common diseases and some integrins have become attractive targets for pharmacological intervention under a number of pathological conditions.[7] Many integrins, including $\alpha_v\beta_3$, $\alpha_v\beta_5$, $\alpha_{IIb}\beta_3$ and $\alpha_5\beta_1$, recognize the tripeptide Arg–Gly–Asp (RGD) motif in their ligands. The observation that $\alpha_v\beta_3$, $\alpha_v\beta_5$ and $\alpha_5\beta_1$ integrin subtypes are essential for tumor angiogenesis and can be successfully inhibited by small-molecule ligands has turned them into attractive targets for cancer research.[8] Control of integrin activity is of crucial

[a]*Università degli Studi di Milano, Dipartimento di Chimica, Via C. Golgi, 19, 20133 Milano, Italy. E-mail: laura.belvisi@unimi.it, donatella.potenza@unimi.it; Fax: +39 (02) 5031 4072; Tel: +39 (02) 5031 4085 or 4086*

[b]*CNR, Istituto di Scienze e Tecnologie Molecolari (ISTM), Via G. Venezian, 21, 20133 Milano, Italy*

[c]*Università degli Studi dell'Insubria, Dipartimento di Scienza e Alta Tecnologia, via Valleggio 11, 22100 Como, Italy*

†Electronic supplementary information (ESI) available: NMR data and computational methods. See DOI: 10.1039/c3ob40540k

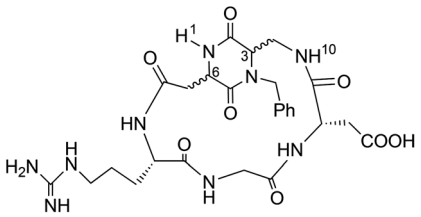

**1** = *cyclo*[(3*S*, 6*S*)DKP-RGD]
**2** = *cyclo*[(3*S*, 6*R*)DKP-RGD]
**3** = *cyclo*[(3*R*, 6*S*)DKP-RGD]

**Fig. 1** Cyclic RGD-peptidomimetics **1–3** containing bifunctional DKP scaffolds.

importance also in platelet aggregation. Indeed, ligand-mimetic therapeutics that inhibit fibrinogen binding to $\alpha_{IIb}\beta_3$ are effective in preventing and treating coronary artery thrombosis. Many peptide and peptidomimetic integrin ligands have been developed, which contain the RGD tripeptide sequence with different flanking residues and three dimensional presentation,[9] and a few potent ligands are actually in different stages of clinical trials for cancer therapy, or in clinical use for antithrombotic therapy.

Notwithstanding these recent achievements, the discovery of new ligands displaying high activity and selectivity together with an optimal pharmacological profile still remains a challenge in this field. In this paper, we report the NMR investigations of the interactions between the cyclic RGD peptidomimetic ligands **1–3** (Fig. 1)[10] and intact ECV304 bladder cancer cells (in which the integrin $\alpha_v\beta_3$ is overexpressed), and platelets (where $\alpha_{IIb}\beta_3$ is predominant). The NMR data were interpreted with the aid of docking calculations thus affording an improved understanding of ligand–integrin interactions.

## Results and discussion

The cyclic peptidomimetics **1–3** expose the RGD sequence and are characterized by bifunctional diketopiperazine scaffolds that differ for the configuration at C-3 and C-6 stereogenic centres (Fig. 1). The different configurations of the scaffolds strongly influence the conformational preferences of the molecules (*vide infra*). Studies by $^1$H-NMR experiments (VT-NMR and NOESY) and Monte Carlo-Stochastic Dynamics (MC-SD) simulations revealed that the ligands **1–3** display well-defined preferred conformations featuring intramolecularly hydrogen-bonded turn motifs stabilized by specific H-bonding patterns.[10a–c]

To investigate the interaction of ligands **1–3** with integrins $\alpha_v\beta_3$ and $\alpha_{IIb}\beta_3$, we performed tr-NOESY and STD NMR experiments‡ with the ligands in a non-deuterated buffer suspension of ECV304 bladder cancer cells and platelets, respectively. The STD spectra of the three ligands **1–3** in the absence of cells did not show any signal; in the presence of cells, an efficient transfer of saturation from the protons of the protein to the ligand was obtained with a 3 second saturation time (60 gaussian pulses, each of 50 ms).

Computational models for the interaction of RGD peptidomimetic ligands **1–3** with the $\alpha_v\beta_3$ integrin were built using our previously developed docking approach,[10b,c] starting from the X-ray structure of the extracellular segment of integrin $\alpha_v\beta_3$ complexed with the cyclic pentapeptide ligand Cilengitide (Protein Data Bank entry 1L5G).[11] In all the calculations, the experimentally observed binding mode of Cilengitide with the $\alpha_v\beta_3$ integrin was taken as a reference model for the analysis of the docking results in terms of ligand–protein interactions. In a similar way, starting from the crystal structure of the integrin $\alpha_{IIb}\beta_3$ headpiece bound to the cyclic heptapeptide Eptifibatide, currently in clinical use to prevent thrombosis (Protein Data Bank entry 2VDN),[12] a docking protocol was developed and applied to study *in silico* the binding of ligands **1–3** to the platelet integrin. The X-ray structures of $\alpha_v\beta_3$ and $\alpha_{IIb}\beta_3$ complexed with RGD ligands have revealed an identical atomic basis for the interaction: RGD binds to the interface of the α and β subunits, the Arg residue fitting into a cleft in the α subunit, and the Asp coordinating a cation in the β subunit. The RGD tripeptide adopts a highly extended conformation across the $\alpha_v\beta_3$ and $\alpha_{IIb}\beta_3$ integrin intersubunit interface. The Arg and Asp side chains extend in opposite directions, and the backbone in between is also extended. Looking at the distinguishing features, the basic ligand side chain must reach further into the deeper β propeller pocket of $\alpha_{IIb}$ to interact with Asp224, whereas the residues Asp150 and Asp218 are nearer in the shallower $\alpha_V$ binding pocket.

### Interactions with ECV304 bladder cancer cells

**Compound 1.** Investigation of the conformational preferences of ligand **1** in the free state by NMR and MC-SD analysis[10b,c] revealed the presence of two main conformations: a Gly–Asp β-turn conformation stabilized by a hydrogen bond between DKP-$NH_{10}$ and Arg–C═O (Fig. 2a), and an Arg–Gly β-turn conformation stabilized by a hydrogen bond between $NH_{Asp}$ and C(8)═O (Fig. 2b). The NOE experiments at 298 K showed two mutually exclusive long-range NOE contacts

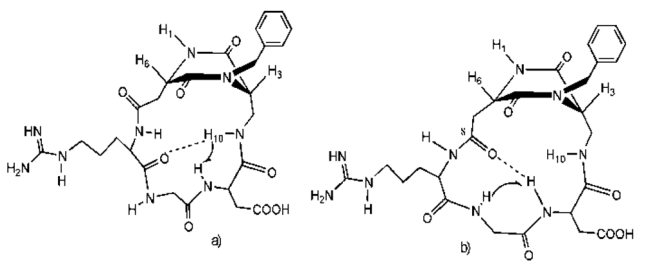

**Fig. 2** Preferred free state conformations of *cis*-DKP-RGD-peptidomimetic **1**. Arrows indicate significant NOE contacts and dotted lines the hydrogen bonding patterns stabilizing β-turn motifs: (a) Gly–Asp β-turn; (b) Arg–Gly β-turn (bound conformation).

‡The spectra were performed on a Bruker Avance 600 MHz. Each sample was prepared in a 3 mm NMR tube with 0.6 mg of a ligand and $6 \times 10^6$ cells in 200 μL of 20 mM phosphate buffer containing additionally 157 mM NaCl, 6 mM KCl and 4 mM $CaCl_2$.

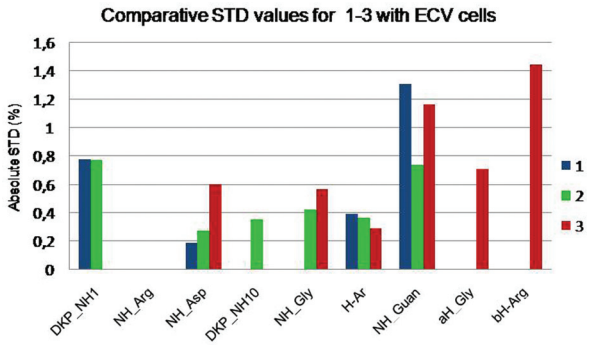


**Fig. 3** Relevant absolute STD percentages for the protons of cyclic DKP-RGD **1–3** obtained at $T$ = 282 K in the presence of ECV304 cells: compound **1** (blue bars), compound **2** (green bars), compound **3** (red bars).

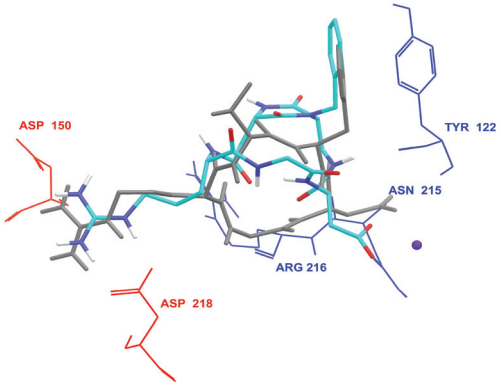


**Fig. 4** Docking best pose of *cis*-DKP-RGD-peptidomimetic **1** (tube representation, C atoms in light blue, N in blue, O in red, H in white) into the crystal structure of the extracellular domain of the $\alpha_v\beta_3$ integrin (α unit red and β unit blue wire representation) overlaid on the bound conformation of Cilengitide (gray tube representation). Only selected integrin residues involved in the interactions with the ligand are shown. The metal ion at MIDAS is shown as a magenta CPK sphere. For the sake of clarity, all H atoms bound to carbon are omitted.

(positive): a cross-peak between DKP-$NH_{10}$ and $NH_{Asp}$ (strong, Fig. 2a), and a cross-peak between $NH_{Gly}$ and $NH_{Asp}$ (medium, Fig. 2b). The tr-NOESY experiment of compound **1** in the presence of ECV304 cells at 298 K also showed positive cross-peaks, which indicate the absence of binding. Lowering the temperature to 282 K, the NOESY spectrum of the free ligand **1** showed cross-peaks with an inverted phase, *i.e.* with the same negative sign as the diagonal. The tr-NOESY spectrum performed at 282 K showed a negative cross-peak between $NH_{Gly}$ (8.82 ppm) and $NH_{Asp}$ (8.13 ppm); this NOE contact is consistent with the β-turn conformation at Arg–Gly stabilized by the hydrogen bond between $NH_{Asp}$ and C(8)═O mentioned above and depicted in Fig. 2b. This would indicate that, upon binding to cells, the conformational equilibrium present in the free state is shifted towards one conformation, and precisely to the less abundant in the free state (Fig. 2b).

To further prove this interaction, STD-NMR experiments were performed in the presence of ECV304 cells at 282 K. In these spectra, the region corresponding to the aromatic and amide protons is well resolved and can be used to measure the absolute intensity of STD (Fig. 3, blue bars). The largest STD effects (1.3% STD absolute intensity) were observed for the guanidine NH protons (7.26 ppm), which are expected to be in contact with the protein. Also the aromatic protons and the DKP-$NH_1$ showed an STD effect (0.4 and 0.8% STD absolute intensity, respectively) and consequently can be considered lying close to the protein surface.

These results are in agreement with the docking analysis of ligand **1** into the $\alpha_v\beta_3$ integrin binding site. Docking studies starting from the bound conformation of compound **1** (Fig. 2b) produced top-ranked poses conserving optimal interactions only between the positively charged Arg guanidinium group of the ligand and the negatively charged side chains of Asp218 and Asp150 in the α unit (Fig. 4). Probably, the short Cβ(Arg)–Cβ(Asp) distance (<8 Å) of this geometry does not allow the simultaneous superimposition of the guanidine and carboxylic groups of the ligand with the corresponding moieties of Cilengitide. In particular, the stabilizing hydrogen bond interactions of Cilengitide carboxylate oxygen with the backbone amides of Asn215 and Tyr122 in the β unit, and the hydrogen bonds between Cilengitide backbone N–H and protein backbone carbonyl groups in the β unit are missing in the poses of compound **1**. In contrast, the ligand benzyl group is suitably positioned to interact with the aromatic moiety of the $\beta_3$-Tyr122, and the DKP-$NH_1$ shows favourable van der Waals contacts with the $\beta_3$-Arg214 side chain (Fig. 4).

**Compound 2.** Conformational studies revealed that, in the free state, ligand **2** adopts mainly one conformation characterized by the presence of a β-turn stabilized by a hydrogen bond between $NH_{Gly}$ and C(5)═O (Fig. 5), and by an extended arrangement of the RGD sequence [Cβ(Arg)–Cβ(Asp) distance of about 9 Å]. NOESY experiments showed a long range contact (positive) between $NH_{Gly}$ and $NH_{Arg}$, confirming this conformation.

The tr-NOESY experiments of compound **2** at 282 K showed negative cross-peaks (*i.e.*, with the same phase as the diagonal), indicating a binding situation. Moreover, the cross-peaks between the aromatic protons and the Arg side chain protons, which can be observed in the NOESY experiments (free ligand), are lacking in the tr-NOESY spectrum (Fig. 6). These cross-peaks suggest folding of the Arg-side chain, which

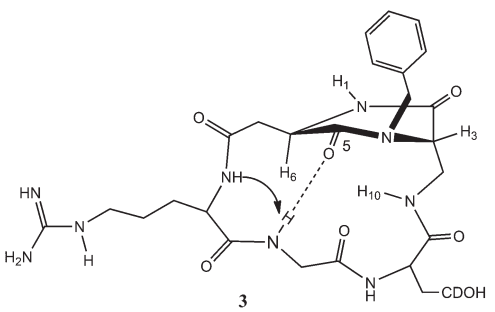


**Fig. 5** Bound conformation of *trans*-DKP-RGD-peptidomimetic **2**. Hydrogen bond (dotted line) and NOE contact (arrow) are indicated.

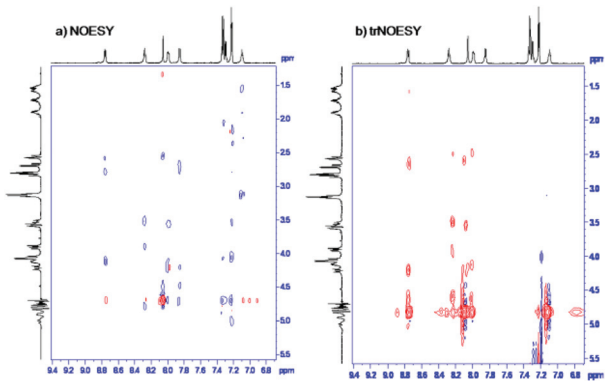


**Fig. 6** Left: NOESY spectrum of free compound **2** in non-deuterated buffer. Right: tr-NOESY spectrum of compound **2** in a cell suspension, reflecting the bound conformation. Experiments performed at $T$ = 282 K.

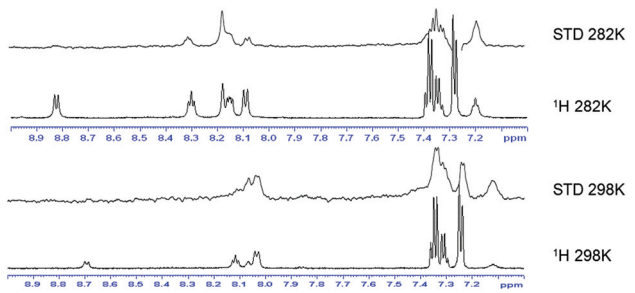


**Fig. 7** STD spectra, $^1$H-NMR spectra (selected regions) of ligand **2** at different temperatures. At $T$ = 298 K, DKP-NH$_1$, NH$_{Asp}$ and NH$_{Gly}$ overlap.

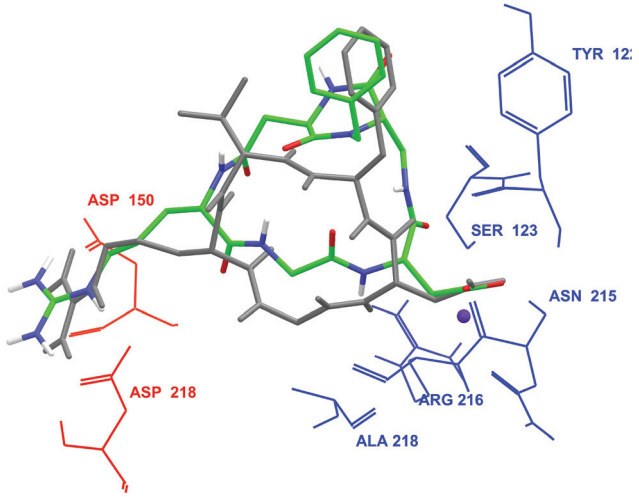


**Fig. 8** Docking best pose of *trans*-DKP-RGD-peptidomimetic **2** (tube representation, C atoms in green, N in blue, O in red, H in white) into the crystal structure of the extracellular domain of an $\alpha_v\beta_3$ integrin ($\alpha$ unit red and $\beta$ unit blue wire representation) overlaid on the bound conformation of Cilengitide (gray tube representation). Only selected integrin residues involved in the interactions with the ligand are shown. The metal ion at MIDAS is shown as a magenta CPK sphere. For the sake of clarity, all H atoms bound to carbon are omitted.

does not occur in the bound ligand. In fact, the formation of the electrostatic clamp inside the binding pocket requires that the side chains of Arg and Asp lie in an extended conformation.

STD-NMR experiments in the presence of the cell suspension were performed both at 298 and 282 K (Fig. 7). At 298 K the signals of DKP-NH$_1$, NH$_{Asp}$ and NH$_{Gly}$ overlap, and therefore it is difficult to assess their involvement in the binding process. The largest STD effect is observed for the guanidine NH protons (7.15 ppm, 2.3% STD absolute intensity). At 282 K (see Fig. 3, green bars) the largest STD effects are observed for DKP-NH$_1$ (0.8% STD absolute intensity) and for the guanidine NH protons (7.26 ppm, 0.7% STD absolute intensity). The aromatic protons, DKP-NH$_{10}$, NH$_{Gly}$ and NH$_{Asp}$, show similar STD effects (0.4, 0.4, 0.4 and 0.3%, respectively) and can also be considered as lying close to the protein surface. Fig. 7 shows the STD and $^1$H-NMR of ligand **2** at both temperatures (298 and 282 K). Temperature is an important parameter for the sensitivity of STD spectroscopy;[13] in fact, it strongly influences the kinetics and the affinity constant of protein–ligand complex formation and, doing so, it affects the observed STD signals.

The signals observed in the STD spectrum confirm that ligand **2** is in an extended conformation when binding to cells, and it interacts closely with both the $\alpha_v$ (by the guanidine NHs) and $\beta_3$ (by NH$_{Asp}$, NH$_{Gly}$, DKP-NH$_{10}$, DKP-NH$_1$ and the aromatic protons) subunits.

These results are in agreement with the docking analysis of ligand **2** into the $\alpha_v\beta_3$ integrin binding site. In fact, docking studies starting from the bound conformation of compound **2** (Fig. 5) produced top-ranked binding modes conserving all the key polar interactions of the X-ray complex. The positively charged guanidinium group of the ligand interacts with the negatively charged carboxylates of Asp218 and Asp150 in the $\alpha$ unit; one carboxylate oxygen of the ligand is coordinated to the metal cation in the metal-ion-dependent adhesion site (MIDAS) region of the $\beta$ unit, while the second carboxylate oxygen forms hydrogen bonds with the backbone amides of Asn215 and Tyr122 in the $\beta$ unit. A further stabilizing interaction involves the formation of a hydrogen bond between the ligand backbone NH of the Asp residue and the backbone carbonyl group of Arg216 in the $\beta$ unit (Fig. 8). Moreover, favourable van der Waals contacts can be detected between the ligand benzyl group and the aromatic moiety of $\beta_3$-Tyr122 and the H$\alpha$ of Ser123, between DKP-NH$_1$ and the terminal methyl protons of $\beta_3$-Met180, between DKP-NH$_{10}$ and the H$\beta$ of Ser123 and the carbonyl group of Tyr122, and between NH$_{Gly}$ and the methyl protons of $\beta_3$-Ala218.

**Compound 3.** Similarly to compound **2**, the free state conformation of ligand **3** is characterized by a β-turn motif stabilized by a hydrogen bond between NH$_{Gly}$ and C(5)=O (Fig. 9), as suggested by the relevant long-range NOE interaction between NH$_{Gly}$ and NH$_{Arg}$ (positive at 298 K and negative at 282 K). In the tr-NOESY experiments at 298 K, the cross-peak intensity is close to zero, while at 282 K the contacts are negative like in the free state.

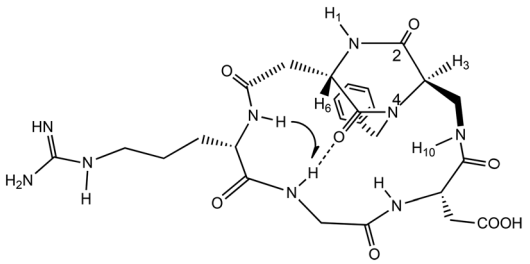

**Fig. 9** Bound conformation of *trans*-DKP-RGD-peptidomimetic **3**. Hydrogen bond (dotted line) and NOE contact (arrow) are indicated.

Also for compound **3** STD-NMR experiments were performed at two temperatures, 298 and 282 K. The experiment at 298 K showed quite large STD effects for the guanidine NH, $NH_{Asp}$ and $NH_{Gly}$ (2.8, 2.0 and 2.1% STD absolute intensity, respectively). When the temperature was lowered from 298 to 282 K, a decreased intensity of STD signals was observed. In fact, at 282 K, the signals for the guanidine NH, $NH_{Asp}$ and $NH_{Gly}$ showed values of 1.2, 0.6 and 0.6% STD absolute intensity, respectively. Additionally, at 282 K, the signals for the aromatic protons, $H\alpha_{Gly}$ and $H\beta_{Arg}$ (0.3, 0.7 and 1.4% STD absolute intensity, respectively), appeared in the STD spectrum (see Fig. 3, red bars).

Docking calculations into the $\alpha_v\beta_3$ integrin binding site, starting from the preferred RGD extended conformation [Cβ(Arg)–Cβ(Asp) distance of about 9 Å] of ligand **3** (Fig. 9), produced top-ranked binding modes conserving a good correspondence with the receptor-bound structure of Cilengitide and all the important polar interactions of the X-ray complex already described for ligand **2**. A relevant difference with the interaction mode of ligand **2** is shown by the benzyl group of ligand **3** which is placed between the side chains of $\beta_3$-Arg214 and $\alpha_v$-Tyr178 (Fig. 10).

***In vitro* biological assays.** Cyclic RGD peptidomimetics **1–3** were examined for their ability to compete with biotinylated vitronectin for binding to the purified $\alpha_v\beta_3$ and $\alpha_v\beta_5$ receptors.[10b,c] The $IC_{50}$ values are collected in Table 1 together with the value of the reference compound *cyclo*(RGDfV).

To assess the activity of compounds **1–3** as integrin antagonists on a cell model, cell adhesion experiments were performed using ECV304 bladder cancer cells, which overexpress integrin $\alpha_v\beta_3$.[4] Cells were allowed to adhere to immobilized fibronectin or vitronectin in the presence of increasing concentrations of the tested compound. As shown in Table 2, *cyclo*-[(3*S*,6*S*)DKP-RGD] **1** (*cis*) was not able to impair the adhesion of the ECV304 cell line on either vitronectin or fibronectin, thus confirming its low affinity for the $\alpha_v\beta_3$ integrin. In contrast, both cyclic peptidomimetics **2** and **3** (*trans*) significantly inhibited cell adhesion to either fibronectin or vitronectin, exhibiting a micromolar anti-adhesive activity. These data further demonstrate that the more extended RGD sequence forced by the *trans* geometry of the diketopiperazine scaffolds of compounds **2** and **3** (compared to a more folded RGD sequence due to the *cis* geometry present in compound **1**) gives rise to a better pre-organization of the cyclic peptidomimetic for binding to the integrin receptors.[10b,c]

The micromolar activities obtained for compounds **2** and **3** in the ECV304 cell adhesion assay represent an ideal range for testing interactions between the ligands and the integral membrane protein of intact cells by means of tr-NOE and STD experiments (*vide supra*).

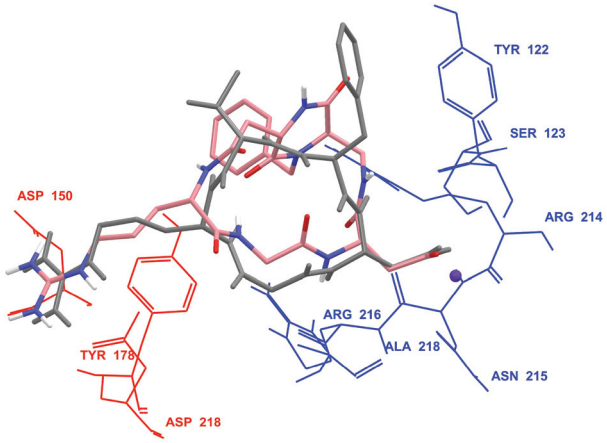


**Fig. 10** Docking best pose of *trans*-DKP-RGD-peptidomimetic **3** (tube representation, C atoms in pink, N in blue, O in red, H in white) into the crystal structure of the extracellular domain of an $\alpha_v\beta_3$ integrin (α unit red and β unit blue wire representation) overlaid on the bound conformation of Cilengitide (gray tube representation). Only selected integrin residues involved in the interactions with the ligand are shown. The metal ion at MIDAS is shown as a magenta CPK sphere. For the sake of clarity, all H atoms bound to carbon are omitted.

**Table 1** Inhibition of biotinylated vitronectin binding to the $\alpha_v\beta_3$ and $\alpha_v\beta_5$ receptors

| Ligand | $\alpha_v\beta_3$ $IC_{50}$ [a] [nM] | $\alpha_v\beta_5$ $IC_{50}$ [a] [nM] |
|---|---|---|
| **1** | 3898 ± 418 | $>10^4$ |
| **2** | 4.5 ± 1.1 | 149 ± 25 |
| **3** | 3.2 ± 2.7 | 114 ± 99 |
| *cyclo*[RGDfV] | 3.2 ± 1.3 | 7.5 ± 4.8 |

[a] $IC_{50}$ values were calculated as the concentration of the compound required for 50% inhibition of biotinylated vitronectin binding as estimated by GraphPad Prism software. All values are the arithmetic mean ± SD of triplicate determinations.

**Table 2** Effect of compounds **1–3** on ECV304 cell adhesion to vitronectin and fibronectin

| Ligand | Vitronectin $IC_{50}$ [a] [μM] | Fibronectin $IC_{50}$ [a] [μM] |
|---|---|---|
| **1** | >200 | >200 |
| **2** | 13.8 ± 0.2 | 2.2 ± 0.4 |
| **3** | 49.5 ± 3.0 | 15.0 ± 3.9 |
| *cyclo*[RGDfV] | 0.22 ± 0.00 | 0.36 ± 0.09 |

[a] Each data point was performed in triplicate in two independent experiments.

### Interactions with platelets

Ligands **1–3** were subsequently analyzed in the presence of platelets which, as already mentioned, express mainly integrin $\alpha_{IIb}\beta_3$.

The tr-NOESY experiments at 298 K gave evidence of binding for ligands **1** and **3**. The conformational equilibrium of compound **1** in the free state (Fig. 2) is apparently unaltered upon binding to platelets. In the case of compound **3**, the cross-peaks between the aromatic protons and the Arg-side chain protons, which can be observed in the NOESY experiments (free ligand), are lacking in the tr-NOESY spectrum. The absence of these cross-peaks in the bound state suggests an extended conformation of the Arg-side chain, suitable for the constitution of the electrostatic clamp. In the case of compound **2**, the experiment is inconclusive since the ligand cross peak intensity was close to zero and the only detectable cross-peaks were related to the platelet membrane.

The STD-NMR experiment on compound **1** in the presence of the platelet suspension displayed signals for the guanidine NH, DKP-$NH_1$ and the aromatic protons (1.0, 0.6 and 0.3% STD absolute intensity, respectively, see Fig. 11, blue bars). These results highlight that compound **1** interacts through its basic moiety with the $\alpha_{IIb}$ subunit of integrin $\alpha_{IIb}\beta_3$. In the case of ligand **2**, the largest STD effect is again observed for the guanidine NH, and with a higher STD value (2.7% STD absolute intensity, see Fig. 11, green bars); hence this proton closely approaches the $\alpha_{IIb}$ subunit of the protein. Remarkably, also DKP-$NH_{10}$, DKP-$NH_1$, $NH_{Gly}$, $NH_{Asp}$ and the aromatic protons of this ligand show quite intense STD effects (2.3, 0.9, 0.8, 0.8 and 0.5%, respectively) and, as a consequence, ligand **2** can be considered as lying close to the protein surface.

A map of the STD signals obtained for ligand **2** in the presence of platelets and ECV cells (Fig. 12) shows that the same protons in both the RGD sequence and the DKP scaffold provide significant STD percentages and, as a consequence, the epitope is conceivably the same.

The STD-NMR results in the presence of platelets are in agreement with the docking analysis of ligand **2** into the $\alpha_{IIb}\beta_3$ integrin binding site. Docking studies starting from the bound

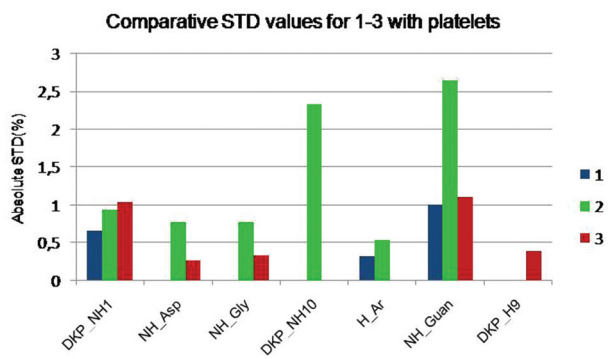


**Fig. 11** Relevant absolute STD percentages for the protons of cyclic DKP-RGD **1–3** obtained at $T$ = 298 K in the presence of a platelet suspension: compound **1** (blue bars), compound **2** (green bars), compound **3** (red bars).

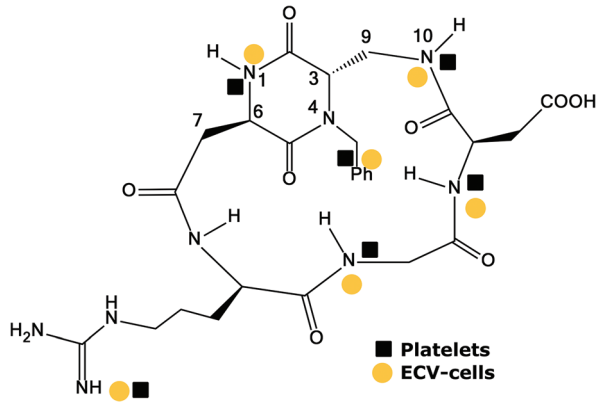


**Fig. 12** Binding epitopes: map of the STD signals of ligand **2** in the presence of platelets (black squares) with respect to ECV cells (orange circles).

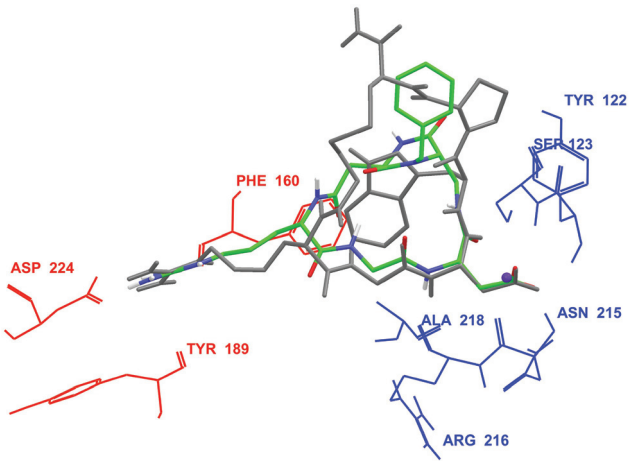


**Fig. 13** Docking best pose of *trans*-DKP-RGD-peptidomimetic **2** (tube representation, C atoms in green, N in blue, O in red, H in white) into the crystal structure of the integrin $\alpha_{IIb}\beta_3$ headpiece (α unit red and β unit blue wire representation) overlaid on the bound conformation of Eptifibatide (gray tube representation). Only selected integrin residues involved in the interactions with the ligand are shown. The metal ion at MIDAS is shown as a magenta CPK sphere. For the sake of clarity, all H atoms bound to carbon are omitted.

conformation of compound **2** (Fig. 5) produced top-ranked binding modes conserving all the key interactions of the X-ray complex between $\alpha_{IIb}\beta_3$ integrin and Eptifibatide (Fig. 13).[12] The guanidine group of the ligand Arg forms a charged hydrogen bond to $\alpha_{IIb}$ residue Asp224 as well as a hydrogen bond to an $\alpha_{IIb}$ backbone carbonyl (Phe160 or Tyr189). The carboxylate of the ligand Asp side chain directly coordinates to the MIDAS cation and is further stabilized by three hydrogen bonds to the $\beta_3$ backbone (Asn215, Tyr122 and Ser123) and one to the $\beta_3$ Asn215 side chain. A further stabilizing interaction involves the formation of a hydrogen bond between the ligand backbone NH of the Asp residue and the backbone carbonyl group of Arg216 in the $\beta_3$ unit. Moreover, favourable van der Waals contacts can be detected between the ligand benzyl group and the aromatic moiety of $\beta_3$-Tyr122 and the Hα of Ser123, between DKP-$NH_1$ and the aromatic protons of $\alpha_{IIb}$-Phe160,

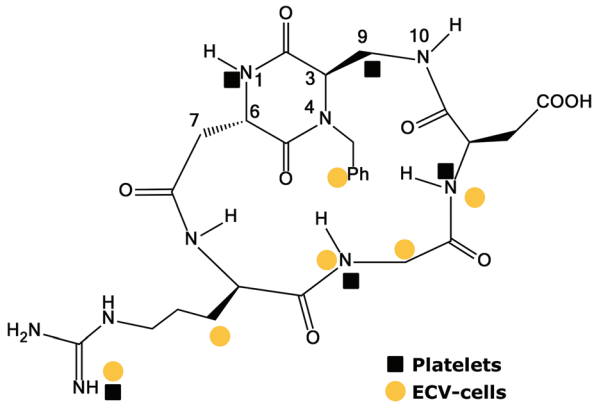


**Fig. 14** Binding epitopes: map of the STD signals of ligand **3** in the presence of platelets (black squares) with respect to ECV cells (orange circles).

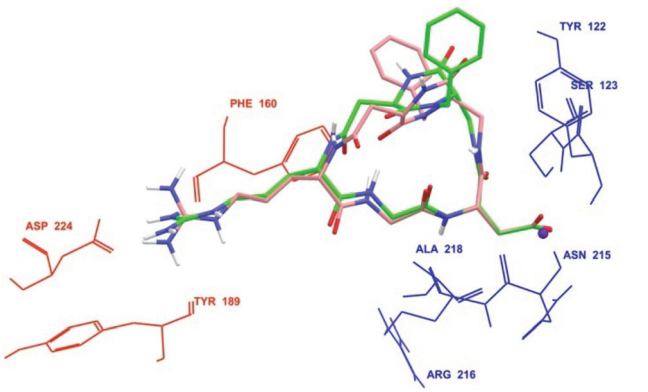


**Fig. 15** Docking best poses of *trans*-DKP-RGD-peptidomimetics **2** and **3** (green and pink atom colour tube representation, respectively) into the crystal structure of the integrin $\alpha_{IIb}\beta_3$ headpiece (α unit red and β unit blue wire representation).

between DKP-$NH_{10}$ and the Hβ of Ser123, and between $NH_{Gly}$ and the methyl protons of $\beta_3$-Ala218. It is worth noting that these contacts have lower mean distance values in the docking poses calculated for $\alpha_{IIb}\beta_3$ than in those found for $\alpha_v\beta_3$.

In the case of compound **3** the protons involved in the interaction with platelets belong to the DKP scaffold (DKP-$NH_1$ and DKP-H9, 1.0 and 0.4% STD absolute intensity, respectively) as well as to the RGD sequence ($NH_{Gly}$, $NH_{Asp}$ and the guanidine NH, 0.3, 0.3 and 1.1% STD absolute intensity, respectively), while the aromatic protons do not appear to be in contact with the protein. These signals are also observed in the interaction with platelets of compound **2**, and therefore the epitopes of compounds **2** and **3** appear to be quite similar while binding to platelets. A different situation is found for the interaction of ligand **3** with ECV304 tumour cells: here only the RGD protons and the aromatic protons of the DKP benzyl group are involved, while the protons of the DKP nucleus are not affected by saturation transfer from the protein (Fig. 14).

Docking calculations into the $\alpha_{IIb}\beta_3$ integrin binding site, starting from the preferred RGD extended conformation of ligand **3** (Fig. 9) produced top-ranked binding modes conserving all the important polar interactions of the X-ray complex with Eptifibatide already described for ligand **2**. Favourable van der Waals contacts can be detected between DKP-$NH_1$ and the Hβ of Ser123, between DKP-H9 and the aromatic protons of $\beta_3$-Tyr122, and between $NH_{Gly}$ and the methyl protons of $\beta_3$-Ala218. A superimposition between the calculated interaction mode of ligands **2** and **3** into the $\alpha_{IIb}\beta_3$ integrin binding site is shown in Fig. 15.

## Conclusions

NMR methodologies based on saturation transfer and detection of transferred NOEs have become powerful tools for the determination of ligand–protein interactions and of the binding epitopes. In this work, we have used these techniques to shed light on the binding epitope of peptidomimetic integrin ligands **1–3** in the interaction with living cells known to express on their membrane integrins $\alpha_v\beta_3$ (ECV304 bladder cancer cells) and $\alpha_{IIb}\beta_3$ (human platelets). The NMR results were supported by docking studies and were compared to the results of competitive $\alpha_v\beta_3$ receptor binding assays (Table 1) and competitive ECV304 cell adhesion experiments (Table 2). The ligands *cyclo*[DKP-RGD] **1–3** are cyclic peptidomimetics containing the RGD sequence and chiral bifunctional diketopiperazine scaffolds, differing for the configuration at C-3 and C-6 stereogenic centres (Fig. 1). The scaffold stereochemistry influences the conformation of the ligands both in the free and in the cell-bound states. In particular, the (3*S*,6*S*)-configuration of ligand **1** imparts a kinked conformation to the RGD sequence which is reflected in the relatively short Cβ(Arg)–Cβ(Asp) distance (<8 Å) and in its low binding affinity to integrin $\alpha_v\beta_3$, as witnessed by the high $IC_{50}$ values in the competitive receptor binding and cell adhesion assays. On the other hand, the *trans* stereochemistry of the DKP side arms in ligands **2** and **3** ensures an extended arrangement of the RGD sequence [Cβ(Arg)–Cβ(Asp) distance of about 9 Å] which is well suited for the $\alpha_v\beta_3$ and $\alpha_{IIb}\beta_3$ integrin receptors. This is reflected in the high binding affinity to the $\alpha_v\beta_3$ integrin receptor and in the efficient ECV304 cell adhesion inhibition displayed by these compounds.

The tr-NOE and STD experiments were run in the presence of ECV304 bladder cancer cells and platelets. These experiments helped identifying the binding epitopes of the peptidomimetics and defining the ligand–integrin bound conformations and the ligand–receptor interactions at a molecular level. We have observed that (i) the primary interaction between the ligand and the receptor is performed by the guanidine residue of the arginine side chain (see behaviour of peptidomimetic **1**), (ii) the extended conformation of the *trans* ligands **2** and **3** ensures the formation of the electrostatic clamp (STD effects on protons of the Arg and Asp residues), (iii) the opposite configuration at C-3 and C-6 stereogenic centres of the DKP scaffold of the *trans* ligands **2** and **3** induces a different binding epitope for the non-RGD moiety of the ligands (diketopiperazine and benzyl substituent). In particular, ligand **2** interacts with ECV304 and platelets through

 

the same binding epitope (see Fig. 12), whereas in the case of ligand **3** a different pattern of STD is observed (the DKP moiety is involved only in the interaction with platelets, and the benzyl group only with ECV cells, see Fig. 14). Finally, these results are well modelled by docking analysis of **1–3** in the active sites of $\alpha_v\beta_3$ and $\alpha_{IIb}\beta_3$ integrin receptors.

In conclusion, the combination of advanced NMR-techniques and computational modelling represents a valuable tool for the investigation of ligand–receptor interactions in living cells.

## Acknowledgements

We thank Milan University for a PhD Fellowship (to I.G.). We also gratefully acknowledge Ministero dell'Università e della Ricerca for financial support (PRIN project 2010NRREPL: Synthesis and biomedical applications of tumor-targeting peptidomimetics). U.P. thanks Fondazione CARIPLO for a research grant (Project: RedDrugTrain).

## Notes and references

1 (*a*) C. Dalvit, *Drug Discovery Today*, 2009, **14**, 1051–1057; (*b*) B. Meyer and T. Peters, *Angew. Chem., Int. Ed.*, 2003, **42**, 864–890.

2 (*a*) B. Meyer, T. Weimar and T. Peters, *Eur. J. Biochem.*, 1997, **246**, 705–709; (*b*) T. Haselhorst, J. F. Espinosa, J. Jimenez-Barbero, T. Sokolowski, P. Kosma, H. Brade, L. Brade and T. Peters, *Biochemistry*, 1999, **38**, 6449–6459; (*c*) M. Mayer and B. Meyer, *J. Med. Chem.*, 2000, **43**, 2093–2099; (*d*) C. B. Post, *Curr. Opin. Struct. Biol.*, 2003, **13**, 581–588.

3 (*a*) S. Mari, D. Serrano-Gómez, F. J. Cañada, A. L. Corbí and J. Jiménez-Barbero, *Angew. Chem., Int. Ed.*, 2005, **44**, 296–298; (*b*) B. Claasen, M. Axmann, R. Meinecke and B. Meyer, *J. Am. Chem. Soc.*, 2005, **127**, 916–919; (*c*) A. Bhunia, S. Bhattacharjya and S. Chatterjee, *Drug Discovery Today*, 2012, **17**, 505–512.

4 D. Potenza, F. Vasile, L. Belvisi, M. Civera and E. M. V. Araldi, *ChemBioChem*, 2011, **12**, 695–699.

5 D. Potenza and L. Belvisi, *Org. Biomol. Chem.*, 2008, **6**, 258–262.

6 (*a*) R. O. Hynes, *Cell*, 2002, **110**, 673–687; (*b*) Y. Takada, X. Ye and S. Simon, *Genome Biol.*, 2007, **8**, 215.

7 M. Shimaoka and T. A. Springer, *Nat. Rev. Drug Discovery*, 2003, **2**, 703–716.

8 C. J. Avraamides, B. Garmy-Susini and J. A. Varner, *Nat. Rev. Cancer*, 2008, **8**, 604–617.

9 (*a*) C. Mas-Moruno, F. Rechenmacher and H. Kessler, *Anti-Cancer Agents Med. Chem.*, 2010, **10**, 753–768; (*b*) L. Auzzas, F. Zanardi, L. Battistini, P. Burreddu, P. Carta, G. Rassu, C. Curti and G. Casiraghi, *Curr. Med. Chem.*, 2010, **17**, 1255–1299.

10 (*a*) A. S. M. Ressurreição, A. Bordessa, M. Civera, L. Belvisi, C. Gennari and U. Piarulli, *J. Org. Chem.*, 2008, **73**, 652–660; (*b*) A. S. M. Ressurreicao, A. Vidu, M. Civera, L. Belvisi, D. Potenza, L. Manzoni, S. Ongeri, C. Gennari and U. Piarulli, *Chem.–Eur. J.*, 2009, **15**, 12184–12188; (*c*) M. Marchini, M. Mingozzi, R. Colombo, I. Guzzetti, L. Belvisi, F. Vasile, D. Potenza, U. Piarulli, D. Arosio and C. Gennari, *Chem.–Eur. J.*, 2012, **18**, 6195–6207; (*d*) R. Colombo, M. Mingozzi, L. Belvisi, D. Arosio, U. Piarulli, N. Carenini, P. Perego, N. Zaffaroni, M. De Cesare, V. Castiglioni, E. Scanziani and C. Gennari, *J. Med. Chem.*, 2012, **55**, 10460–10474.

11 J.-P. Xiong, T. Stehle, R. Zhang, A. Joachimiak, M. Frech, S. L. Goodman and M. A. Arnaout, *Science*, 2002, **296**, 151–155.

12 (*a*) T. Xiao, J. Takagi, B. S. Coller, J.-H. Wang and T. A. Springer, *Nature*, 2004, **432**, 59–67; (*b*) T. A. Springer, J. Zhu and T. Xiao, *J. Cell Biol.*, 2008, **182**, 791–800.

13 P. Groves, K. E. Kövér, S. André, J. Bandorowicz-Pikula, G. Batta, M. Bruix, R. Buchet, A. Canales, F. J. Cañada, H. J. Gabius, D. V. Laurents, J. R. Naranjo, M. Palczewska, S. Pikula, E. Rial, A. Strzelecka-Kiliszek and J. Jiménez-Barbero, *Magn. Reson. Chem.*, 2007, **45**, 745–748.